Optimization of $K\alpha$ bursts for photon energies between 1.7 and 7 keV produced by femtosecond-laser-produced plasmas of different scale length

Ch. Ziener,* I. Uschmann, G. Stobrawa, Ch. Reich, P. Gibbon,† T. Feurer,‡ A. Morak, S. Düsterer, H. Schwoerer, E. Förster, and R. Sauerbrey

Institut für Optik und Quantenelektronik, Friedrich-Schiller-Universität Jena, Max-Wien-Platz 1, 07743 Jena, Germany

(Received 12 January 2001; revised manuscript received 20 March 2001; published 26 June 2002)

The conversion efficiency of a 90 fs high-power laser pulse focused onto a solid target into x-ray $K\alpha$ line emission was measured. By using three different elements as target material (Si, Ti, and Co), interesting candidates for fast x-ray diffraction applications were selected. The $K\alpha$ output was measured with toroidally bent crystal monochromators combined with a GaAsP Schottky diode. Optimization was performed for different laser intensities as well as for different density scale lengths of a preformed plasma. These different scale lengths were realized by prepulses of different intensities and delay times with respect to the main pulse. Whereas the $K\alpha$ yield varied by a factor of 1.8 for different laser intensities, the variation of the density scale length could provide a gain factor up to 4.6 for the $K\alpha$ output.

DOI: 10.1103/PhysRevE.65.066411 PACS number(s): 52.38.−r, 52.25.Os, 52.70.La, 41.50.+h

I. INTRODUCTION

X-ray bursts from subpicosecond-laser plasmas were discussed many years ago as a probe source to study fast processes in matter [1,2]. It has been successfully demonstrated that $K\alpha$ bursts of femtosecond-laser plasmas can be used in fast x-ray diffraction experiments to study the temporal response of x-ray diffraction from crystals [3–6]. For investigations of fast temporal processes like chemical reactions, it is essential to develop an efficient, bright x-ray source in the usual photon energy region used for structural analysis between 4 and 20 keV. This is particularly important for extending this method to a higher sensitivity and to other samples like molecules and clusters. In contrast to lasers with pulse durations of several hundred picoseconds or even nanoseconds, the focused laser intensities of current short-pulse lasers can easily reach values above 5.0×10^{17} W/cm^2 [7]. Such intensities are many orders of magnitude above the plasma formation threshold of a solid, and thus a plasma is created in front of the solid target. The thickness of the created plasma layer is of the order of the penetration depth of the laser radiation in the target material, which ranges from a few tens up to a few hundreds of nanometers. Since a typical plasma expansion velocity is 0.1 nm/fs, no significant hydrodynamic motion occurs during the laser pulse for pulse durations shorter than 100 fs. This means that the laser interacts with a plasma of almost solid density and the plasma density gradient is much smaller than the laser wavelength. There are different absorption mechanisms for these very high intensities. While for lower intensities the laser pulse is coupled into the plasma mainly by collisional absorption (inverse bremsstrahlung), for the short-pulse laser interaction at higher intensities ($>10^{16}$ W/cm^2) collective processes like resonance absorption or vacuum heating become more important [8–10]. A detailed theoretical analysis of the different absorption mechanism is given by Gibbon and Förster [11]. The kind of mechanism that dominates and how efficiently the laser pulse is coupled into the plasma depend mainly on the electron density gradient in front of the solid target, the so-called density scale length:

$$L=\left[\frac{1}{n_e}\left(\frac{dn_e}{dx}\right)\right]^{-1}. \tag{1}$$

More generally used is the reduced scale length $L_\lambda = L/\lambda_L$, with λ_L being the laser wavelength.

A significant amount of the absorbed laser energy can be converted to accelerated electrons with energies of up to 1 MeV [12]. These electrons lose their energy in the solid target, producing bremsstrahlung and characteristic line radiation. The conversion of laser light into x-ray line radiation ($K\alpha$) produced by hot electrons depends on the interaction of the subpicosecond laser pulse with the solid target. Such behavior has been studied experimentally for medium intensities of 4.0×10^{16} W/cm^2, showing that the absorption of the laser pulse, the production of the hot electrons as well as the production of the silicon $K\alpha$ line depend on the plasma scale length created by a prepulse [13]. Other influences for the conversion of a 100 fs laser pulse into $K\alpha$ radiation between 4 and 50 keV have been studied via detailed theoretical analysis by Reich *et al.* [14]. They conclude that the conversion efficiency depends on the laser intensity, i.e., there is an optimal hot electron temperature for creating efficient $K\alpha$ radiation and at the same time avoiding strong reabsorption of the radiation in the target. This analysis was performed for a fixed scale length L of $L/\lambda_L=0.3$, $\lambda=800$ nm.

The x-ray lines investigated in the present work were selected under the following considerations as candidates for time-resolved x-ray diffraction or other applications. The Si

*Present address: Central Laser Facility, Rutherford Appleton Laboratory, Chilton Didcot, OX11 0QX, United Kingdom. Email address: c.ziener@rl.ac.uk

†Present address: Forschungszentrum Jülich GmbH, Zentralinstitut für Angewandte Mathematik (ZAM), D-52425 Jülich, Germany.

‡Present address: Department of Chemistry, The Massachusetts Institute of Technology, Cambridge, MA 02139-4208.

$K\alpha$ line which has the longest wavelength undergoes high absorption and therefore has a small penetration depth of about 1 μm compared to $K\alpha$ lines with shorter wavelengths. This property is essential to match the small interaction depth (skin or absorption depth) of the pumping laser with the x-ray penetration depth, when, for instance, a crystalline sample is heated by a laser. Furthermore, such soft x-ray lines are standard sources for x-ray-induced photoelectron spectroscopy of surfaces. On the other hand, the Si $K\alpha$ line can only be used for a few selected crystalline materials, because the double lattice plane distance has to be greater than the wavelength in order to fulfill the Bragg condition. Therefore x-ray lines at shorter wavelengths are essential for time-resolved diffraction. To work with almost all crystalline samples a $K\alpha$ line from heavier elements like titanium or cobalt has to be used.

For the optimization of the electron energy it is important to consider that the *K*-shell cross section of electrons is maximal if the electron energy is about three times the binding energy of the *K*-shell electron. These binding energies are 1.74, 4.51, and 6.93 keV for the case of Si, Ti, and Co, respectively. This means that most of the hot electrons produced by the laser should have their energy in the range 6–28 keV. The fluorescence yield, which gives the ratio between fluorescence radiation and Auger decay processes, strongly increases with atomic number Z ($Z=14$, 0.0504; $Z=21$, 0.225; $Z=27$, 0.388) and should yield a similar $K\alpha$ conversion, despite the fact that a much higher energy is needed for *K*-shell excitation of high-Z elements.

In this paper we have measured the emitted photon numbers of the three $K\alpha$ lines mentioned above. The plasma scale length was modified by a laser prepulse at various delay times relative to the laser main pulse. For the Si $K\alpha$ line the conversion was measured for different main pulse intensities as well as different prepulse intensities as a function of the delay between prepulse and main pulse. For the Ti $K\alpha$ and the Co $K\alpha$ lines the intensity of the main pulse was varied, keeping the prepulse intensity fixed at its highest value.

II. EXPERIMENTAL SETUP

A schematic drawing of the main parts of the experimental setup (the prepulse unit together with the focusing and the x-ray optics) is shown in Fig. 1.

The experiment was performed with the Jena multiterawatt Ti:sapphire laser. This chirped-pulse-amplification laser system consists of an oscillator, a stretcher, a regenerative amplifier, two additional multipass amplifiers, and a vacuum compressor. The maximum energy is 1.3 J before the compressor. This leads to about 1 J after the compressor with a pulse duration of 80 fs at a repetition rate of 10 Hz. After the vacuum compressor the laser beam is guided to the target chamber inside a vacuum beamline. In the vacuum chamber the beam is focused by an off-axis parabolic mirror onto various solid targets. In our experiment we used a maximum energy of 240 mJ with a pulse duration (full width at half maximum) of 90 fs. The temporal structure of the laser pulse was measured by a third-order multishot autocorrelator with

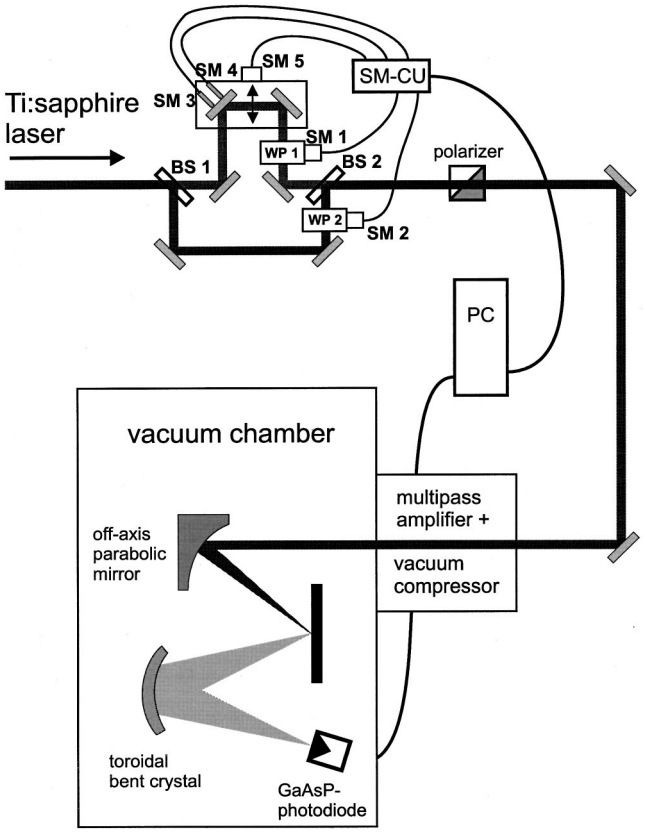

FIG. 1. Experimental setup for the measurement of the $K\alpha$ radiation, showing the unit for the generation of a defined prepulse and the focusing arrangement in the target chamber with the x-ray optics and the detector.

a dynamic range of four orders of magnitude. There are two prepulses at 4 ps and 600 fs before the main pulse, having an intensity contrast ratio of 2×10^{-4} and 5×10^{-3}, respectively. No other prepulses with a contrast ratio bigger than 10^{-4} were detected within 200 ps before the main pulse. The contrast ratio in the time domain 2 ns and more before the main pulse was measured using a fast photodiode with filters. Parasitic prepulses were measured to be less than 5×10^{-6} times the energy of the main pulse. The energy within the focal spot was measured in two steps. First the focused beam was sent through a pinhole with a diameter of 50 μm and the transmitted energy was measured. Following that a region of size 100×100 μm^2 around the focus was imaged onto a 16-bit charge-coupled device camera. 35% of the energy incident on the parabolic mirror was within a spot of 10×12 μm^2, giving an intensity of 5.0×10^{17} W/cm^2 for a laser energy of 240 mJ.

In order to investigate the interaction of the high-intensity laser pulses with a plasma of a certain scale length, one needs an additional laser pulse to create the preplasma. For this purpose we implemented a prepulse device in our laser amplifier chain. Details of the setup are described elsewhere [15]. The prepulse device is located between the regenerative and the first multipass amplifier. The beam leaving the regenerative amplifier is split into two beams at the beam splitter

TABLE I. Important parameters of the $K\alpha$ measurement for target materials with different atomic numbers Z: crystal reflection of the toroidally bent crystals, the Bragg angle, and the integrated reflectivity.

Z	Photon energy (keV)	Crystal reflection	Bragg angle	Integrated reflectivity (μrad)
14	1.740	Quartz $(10\bar{1}0)$	56.9°	55.0
22	4.505	Silicon (311)	57.0°	28.9
27	6.930	Quartz $(40\bar{4}0)$	57.2°	11.2

(BS1) so that 90% of the energy is reflected as the main beam. Both beams are then sent through rotatable half-wave plates (WP1 and WP2) and superimposed on a second beam splitter (BS2), which is identical to the first one. The maximum energy of the prepulse is about 2% of the maximum energy of the main pulse. The plane of polarization of both beams after the first beam splitter can be adjusted by turning the respective half-wave plate by means of stepping motors (SM1 and SM2). A polarizer after the prepulse unit transmits only the part of the beam with horizontal polarization. In this way the main pulse as well as the prepulse can be attenuated by more than one order of magnitude. The energies of both pulses can be varied independently. The prepulse is sent through an optical delay line giving a temporal distance between prepulse and main pulse in the range of -350 to 100 ps with an accuracy of 6 fs. This accuracy is determined by the step size of stepping motor SM5 which drives the translation stage. A negative delay means that the prepulse arrives on target before the main pulse. To get a good spatial overlap of both focused laser beams one mirror in the optical delay line can be turned around the horizontal and vertical axes by means of two stepping motors (SM3 and SM4). The spatial overlap is automatically corrected over the whole range of the translation stage with an accuracy better than 1.5 μm if the laser beam is focused by an off-axis parabolic mirror with a focal length of 102 mm. All stepping motors are controlled by a computer by means of a stepping motor control unit (SM-CU). The programs are written in LABVIEW (National Instruments).

The $K\alpha$ radiation was selected and refocused by the Bragg reflection off toroidally bent crystals [16]. The crystals have a horizontal bending radius of 150 mm and a vertical bending radius of 106.4 mm. For silicon $K\alpha$ radiation a quartz crystal with $(10\bar{1}0)$ orientation was used. The same crystal but in a fourth-order reflection was used to measure cobalt $K\alpha$ radiation. For the titanium $K\alpha$ radiation a Si crystal with (311) orientation was used. For all cases the Bragg angle was between 56.8° and 57.4°. Considering the focal length in the horizontal and vertical directions and the Bragg angle, almost no astigmatism occurs for the Bragg angles used [17]. The focus size of the $K\alpha$ source produced by the bent crystals is therefore about 100 μm. The x-ray detector consisted of a GaAsP Schottky photodiode protected with a 7 μm Be window [18]. The x-ray source and the photodiode were placed on the Rowland circle of the crystals. The spectral range covered by the crystal is then of the order of the $K\alpha$ linewidth. To calculate the number of photons emitted by the source from the number of photons detected one can use the following equation [16]:

$$N_S = N_{\mathrm{det}} \frac{4\pi}{\Omega} \frac{\Delta\lambda/\lambda}{R_i \cot\Theta_B}. \tag{2}$$

The solid angle covered by the bent crystal is Ω and $\Delta\lambda/\lambda$ is the relative $K\alpha$ linewidth. The integrated reflectivity R_i of the various bent crystals was measured with synchrotron radiation and with an x-ray tube. Table I shows the data for the crystals used in our experiment. The responsiveness of the photodiode was compared with the known quantum efficiency of a Na(Tl) J Scintillator.

Polished massive targets were used which could be moved from shot to shot to use fresh material for each shot. The incident angle of the p-polarized laser pulse was 45°. The observation angle of the crystals was about 40°.

III. RESULTS

The experimental data are presented in the following way. All measured results present the $K\alpha$ signal per laser shot as a function of the delay time between the pre- and the main laser pulse. For better statistics all measurements were repeated five times. The minimum and the maximum were removed from the analysis and the remaining three values were used to determine the mean value. The error bars in the figures are the mean error.

It is possible to determine the absolute photon number or conversion efficiency with the help of Eq. (2). The error in determining the absolut photon number is rather large (about 20%), and thus we did not do it for each experiment. Since we wanted to show the dependence of the $K\alpha$ signal on the main pulse delay, we preferred to show the diode signal with the errors explained above. In the discussion we calculated the absolute photon numbers in the case of the best conversion efficiency.

A. Prepulse intensity for the Si $K\alpha$ line

For the highest achievable main laser intensity of 5.0×10^{17} W/cm^2 the Si $K\alpha$ line radiation was measured for four different prepulse intensities between 2.5×10^{14} and 1.0×10^{16} W/cm^2 (Fig. 2). At the lowest prepulse intensity of 2.5×10^{14} W/cm^2 a small maximal gain of 1.16 was measured at a time delay of -70 ps as well as at -175 ps. We define gain as the efficiency of $K\alpha$ production with a prepulse divided by the efficiency without a prepulse. Al-

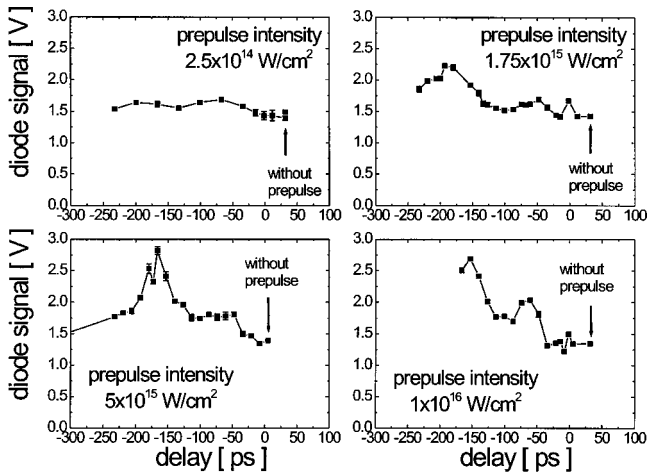

FIG. 2. $K\alpha$ signal as a function of the prepulse delay for various prepulse intensities and a main pulse intensity of 5.0×10^{17} W/cm^2 for silicon as target material.

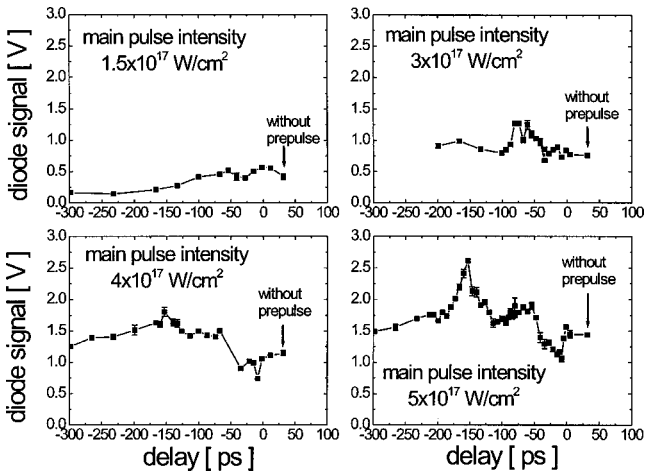

FIG. 3. $K\alpha$ signal as a function of the prepulse delay for various main pulse intensities and a prepulse intensity of 1.0×10^{16} W/cm^2 for silicon as target material.

though the reproducibility of the measurement was very good (the error bars are smaller than the data points in the figure) this gain might not be significant. However, for higher prepulse intensities the two significant maxima are considerably enhanced. The enhancement is greater for the maximum at -175 ps than for the maximum at -70 ps. A maximum gain of 2 was measured for prepulse intensities of 5.0×10^{15} and 1.0×10^{16} W/cm^2. Given the fact that for a decreasing prepulse intensity the output of the Si $K\alpha$ radiation could not be enhanced, the measurements for the other $K\alpha$ lines at higher photon energies were performed only for the highest prepulse intensity of 1.0×10^{16} W/cm^2.

B. Main pulse intensity

1. Silicon Kα (1.740 keV)

The intensity of the main pulse was varied between 1.5×10^{17} and 5.0×10^{17} W/cm^2 by changing the laser energy. The $K\alpha$ photon numbers observed without prepulse at these different laser intensities increase by a factor of 3.7 (Fig. 3). This means that the conversion efficiency of laser energy into $K\alpha$ energy does not vary significantly. Varying the prepulse results in different changes of the $K\alpha$ line output at different main pulse intensities. For the lowest intensity of 1.5×10^{17} W/cm^2 a slight enhancement of the Si $K\alpha$ radiation was observed if the prepulse arrives at the same time as the main pulse. This can be explained by a significant Si $K\alpha$ production of the prepulse. For a prepulse intensity of 1.0×10^{16} W/cm^2 the fraction of laser energy of the prepulse is 7%. Increasing the delay at the lowest main pulse intensity results in a reduction of the $K\alpha$ line output down to 25% of the output without prepulse at -220 ps delay time. By contrast, a clear enhancement of the $K\alpha$ line emission was measured for larger main pulse intensities. The highest gain of about 2 was determined for the main intensity of 5.0×10^{17} W/cm^2 at -150 ps delay time. For these parameters a maximum absolute conversion of laser energy into $K\alpha$ line radiation energy of 1.5×10^{-5} was measured. It is interesting to see the two clear maxima at a main pulse intensity of 5.0×10^{17} W/cm^2. There is also a clear minimum of the $K\alpha$ signal for delays around -50 ps.

2. Titanium Kα (4.505 keV)

The main intensity was varied in the same way as for the Si $K\alpha$ measurement. Comparing the $K\alpha$ photon number observed without prepulse for laser intensities increasing by a factor of 3.3, one can see that the x-ray line output increases by a factor of 6 (see Fig. 4). Notably, for the two highest intensities the conversion efficiency of laser energy into $K\alpha$ energy increases from 5.2×10^{-6} to 8.2×10^{-6}. Again, the influence of the prepulse with an intensity of 1.0×10^{16} W/cm^2 is much more significant for higher main pulse intensities. While no positive gain can be seen for the lowest main pulse intensity of 1.5×10^{17} W/cm^2, a significant enhancement up to 1.9 is visible for the higher intensities. Depending on the delay between the prepulse and the

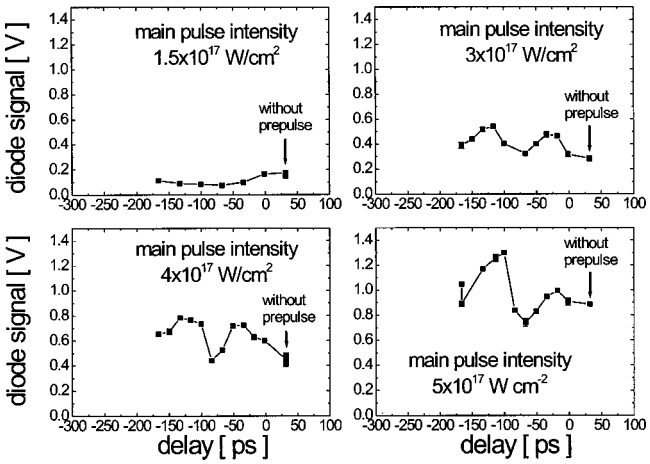

FIG. 4. $K\alpha$ signal as a function of the prepulse delay for various main pulse intensities and a prepulse intensity of 1.0×10^{16} W/cm^2 for titanium as target material.

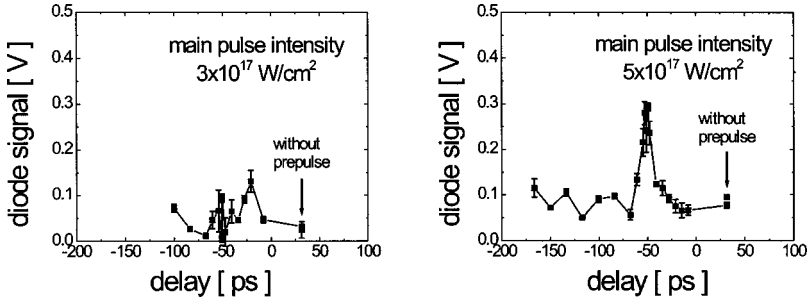

FIG. 5. $K\alpha$ signal as a function of the prepulse delay for various main pulse intensities and a prepulse intensity of 1.0×10^{16} W/cm^2 for cobalt as target material.

main pulse, the $K\alpha$ signal shows two maxima at around -30 and -120 ps and a minimum at around -75 ps. Comparing the conversion of laser energy into $K\alpha$ energy, a maximum absolute conversion of 1.2×10^{-5} was measured for the highest main pulse intensity of 5.0×10^{17} W/cm^2 and a prepulse delay of -100 ps.

3. Cobalt Kα (6.930 keV)

For the Co $K\alpha$ line measurement two main pulse intensities were used with 3.0×10^{17} and 5.0×10^{17} W/cm^2. The $K\alpha$ photon number increases by a factor of 2.9 while the laser intensity was increased only by a factor of 1.7, if no prepulse was used. Because the bremsstrahlung yield increases with Z^2 (Z being the atomic number of the element), the $K\alpha$ signal of the diode was superimposed on a continuum of x rays. To remove the influence of the bremsstrahlung background the signal was measured twice, first at the Bragg position of the $K\alpha$ line and second nearby the peak when only bremsstrahlung was reflected onto the diode. The bremsstrahlung signal comprised up to 50% of the total signal. The difference of the two signals, which is the $K\alpha$ signal, is presented in Fig. 5. A significant gain of 3.44 was measured for the higher intensity of 5.0×10^{17} W/cm^2 at a delay time of -50 ps. Furthermore, a gain of 4.64 was determined for the intensity of 3.0×10^{17} W/cm^2 at -25 ps delay. The maximum absolute conversion is then 0.74×10^{-5} at 5.0×10^{17} W/cm^2 and a delay of -50 ps.

C. Discussion

It was shown in Ref. [13] that it is possible to increase the efficiency of the $K\alpha$ production of a silicon target by using an artificial prepulse some picoseconds before the main laser pulse. For longer prepulse delays the efficiency drops steadily. This behavior was explained by the dependence of resonance absorption on the electron density scale length.

Our experiments, however, show a completely different dependence of the $K\alpha$ yield on the prepulse delay. For the smallest main pulse intensity of 1.5×10^{17} W/cm^2 there is no enhancement with an additional prepulse. For an explanation we need to know the exact temporal structure of our laser pulse and the resulting plasma scale lengths to undertake simulations of the plasma expansion and subsequent $K\alpha$ production.

We did such simulations in several steps. First, a one-dimensional particle-in-cell (PIC) code was used to determine the electron energy spectrum. As input for the PIC calculations the scale length of the electron density was approximated with an exponential decay or was calculated directly with the hydrodynamic code MEDUSA [19]. By means of a Monte Carlo transport code [20] the electron trajectories inside the target were calculated. These simulations were made by taking into consideration the $K\alpha$ ionization cross sections [21] as well as fluorescence yield, relative line intensities, and self-absorption lengths for $K\alpha$ radiation [22].

The results of the simulations are shown in Fig. 6. Parameters used were a laser energy of 240 mJ, an intensity of 5.0×10^{17} W/cm^2, pulse length of 60 fs, and p polarization. The angle of incidence was 45°. The program package allows for the calculation of absolute photon numbers; therefore the calculated efficiency plotted in Fig. 6 is shown as $K\alpha$ photons per steradian.

One can clearly see that for all target materials the efficiency of the $K\alpha$ production is a maximum for a reduced scale length of about 0.2. A remarkable fact is that the $K\alpha$ efficiency is highest for cobalt, although the number of electrons with sufficient energy to create K-shell holes decreases with increasing $K\alpha$ energy. The increase in efficiency is due to the higher reabsorption of the $K\alpha$ radiation for smaller $K\alpha$ energies. For an intensity of 5.0×10^{17} W/cm^2 the $K\alpha$ production is therefore least efficient for titanium and not for cobalt as expected from the pure $K\alpha$ generation. The discrepancy with our measurements will be explained in the next section.

For an estimation of the scale lengths during our experiments the inherent prepulses of our laser system are important. By means of the hydrodynamic code MEDUSA, the reduced electron density scale length was calculated after the

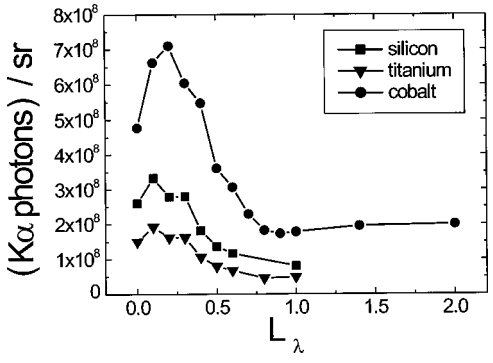

FIG. 6. Calculated absolute photon numbers as a function of the reduced electron density scale length for the three investigated target materials. Parameters are a laser energy of 240 mJ, an intensity of 5.0×10^{17} W/cm^2, a pulse length of 60 fs, an angle of incidence of 45°, and p polarization.

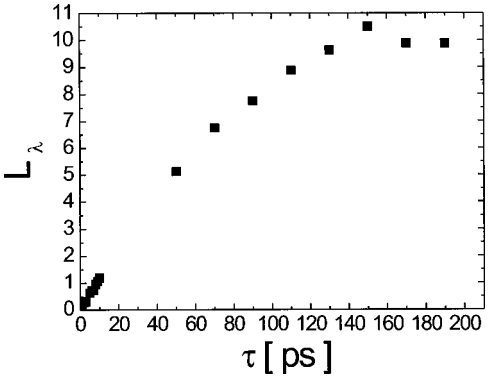

FIG. 7. Reduced electron density scale lengths for large prepulse delays, calculated with MEDUSA.

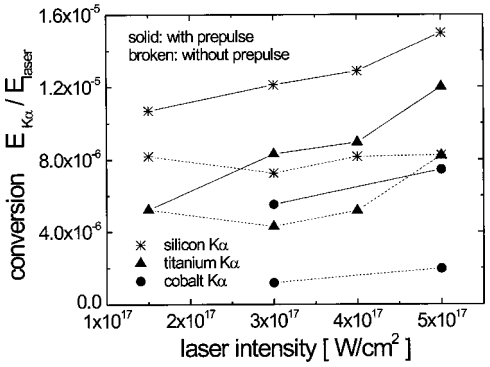

FIG. 8. Conversion efficiencies as a function of the main pulse intensity for silicon, titanium, and cobalt.

interaction of two prepulses with 1.0×10^{14} and 2.5×10^{15} W/cm^2 and delays of -4.1 and -0.6 ps, respectively, with a solid target. The scale lengths are 0.15 for silicon, 0.11 for titanium, and 0.1 for cobalt. Compared with Fig. 6 it is evident that the prepulse structure of our laser pulse is in fact already optimal for efficient $K\alpha$ production. This one-dimensional hydrodynamic code can be used despite the relatively small focal spot diameter (10 μm), because the expansion of the plasma is for these short times much smaller than the lateral plasma diameter.

However, the increase in $K\alpha$ yield for prepulse delays of several tens of picoseconds cannot be explained by the creation of an optimal scale length for resonance absorption as shown in Fig. 7. For prepulse delays of several tens of picoseconds the scale length is more than a factor of 10 larger than the optimum predicted in Fig. 6. Due to the three-dimensional expansion of the plasma, the actual scale length might be smaller by a factor of 3, but even then the scale length would be much too large for prepulse delays in excess of 100 ps.

One possible explanation for the increase in $K\alpha$ yield for large prepulse delays is relativistic self-focusing [23], for which there is a well-known critical power P_{cr}, given by [24]

$$P_{\mathrm{cr}}\sim 17(\omega_L/\omega_p)^2 \ \ \mathrm{GW}, \tag{3}$$

with ω_L the laser and ω_p the plasma frequency. That is, for a laser power of about 2.5 TW, relativistic self-focusing should be possible for electron densities 100 times smaller than the critical density, which for Ti:sapphire lasers is about 2×10^{21} cm^{-3}.

The ''self-focusing length'' z_c is the distance over which the laser beam will reduce its diameter to about the laser wavelength [25,26]:

$$z_c=\frac{z_R}{(P_L/P_{\mathrm{cr}}-1)^{1/2}}, \tag{4}$$

with z_R being the Rayleigh length of the focused laser beam. Obviously, z_c depends on the electron density through P_{cr}. It decreases with increasing electron density. In our experiments the extension of the preplasma should be large enough to enable relativistic self-focusing as demonstrated previously by Borghesi *et al.* [27]. In this paper it was shown experimentally and in simulations that, for plasma densities, scale lengths, and laser power very similar to those used in our experiment, relativistic self-focusing takes place over distances of several tens of wavelengths. There are a number of experiments in which the electron density of an expanding plasma was measured some hundreds of picoseconds [28,29] or several nanoseconds [30] after the heating prepulse. In [29] Fuchs *et al.* measured that for a prepulse intensity of 5×10^{12} W/cm^2 the preplasma with a density above 10^{20} cm^{-3} was extended over more than 300 μm after 500 ps. These measurements show that in our case the preplasma should be extended over at least some tens of micrometers, thus allowing for relativistic self-focusing.

In the case of relativistic self-focusing the laser intensity can be amplified by at least an order of magnitude [31]. Therefore the resulting ponderomotive steepening of the electron density profile [32] would be much higher than in the ''normal'' case and the coupling of the laser light into the plasma is enhanced at the critical density. Also possible is acceleration of additional electrons within the relativistic

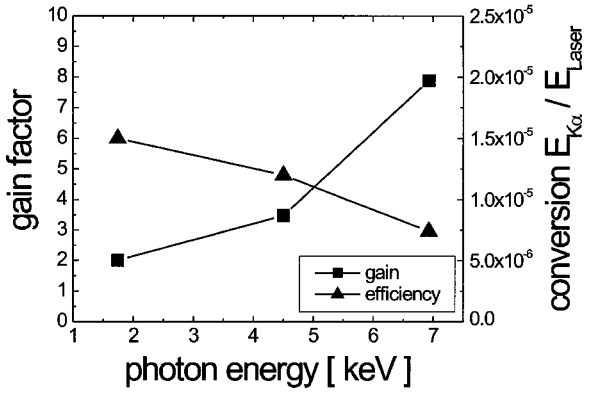

FIG. 9. Potential increase of the $K\alpha$ yield due to an artificial prepulse and optimized laser intensity and the maximum absolute conversion efficiency from laser-into-$K\alpha$ energy for different $K\alpha$ lines (target materials).

channel in the underdense plasma [33], which would also be capable of producing $K\alpha$ radiation.

IV. CONCLUSION

We investigated the efficiency of the production of $K\alpha$ radiation as a function of prepulse delay and main pulse intensity for three different target materials or $K\alpha$ energies.

If the main pulse laser intensity was increased without using a prepulse the conversion $E_{K\alpha}/E_{\text{laser}}$ did increase for titanium and cobalt but not for silicon (Fig. 8). This agrees qualitatively with the results of Eder *et al.* [34] and with the model proposed by Reich *et al.* [14], who both found an optimal intensity for $K\alpha$ production. In our experiment the optimal intensity is probably reached for silicon, not for titanium and cobalt. The reason that the intensity proposed in [14] is smaller than the one measured by us can be explained by the intensity distribution in the present experiment. Only 50% of the laser energy is focused within the focal spot, the remaining part is focused to a lower intensity but over a larger area, producing lower-energy electrons. This might also explain the fact that the conversion efficiency is highest for silicon and not for cobalt as predicted by the simulations in the previous section.

Comparing the gain curves and the conversion efficiencies produced with a prepulse for the three different $K\alpha$ lines, a clear enhancement is visible for all elements investigated. The maximum gain was determined for Co with 4.6, for Ti with 1.9, and for Si with 1.8. At the laser intensities used the maximum gain seems to be more significant for higher photon energies. Considering both effects, the higher conversion efficiency induced by the optimized main pulse laser intensity and the gain due to the scale length variation, a maximum gain of 7.8 was measured for Co $K\alpha$. Comparing the maximal conversion $E_{K\alpha}/E_{\text{laser}}$ for the different $K\alpha$ energies, its value decreases for higher-Z elements by a factor of 2 (Fig. 9). Comparing the gain curves of the different $K\alpha$ energies, the time delay for the maximum gain is shifted toward shorter delays between prepulse and main pulse for elements with a larger Z. In summary, for higher-Z elements the conversion decreases but the optimization by main pulse intensity and scale length variation becomes much more important (Fig. 9).

[1] M. M. Murnane, H. C. Kapteyn, M. D. Rosen, and R. W. Falcone, Science **251**, 531 (1991).

[2] C. P. J. Barty, J. Che, T. Guo, B. Kohler, C. Le Blanc, M. Messina, F. Ráski, C. Rose-Petruck, J. A. Squier, K. Wilson, V. V. Yakovlev, and K. Yamakawa, Proc. Photochem. **30**, 531 (1995).

[3] C. Rischel, A. Rousse, I. Uschmann, P.-A. Albouy, J.-P. Geindre, P. Audebert, J.-C. Gauthier, E. Förster, J.-L. Martin, and A. Antonetti, Nature (London) **390**, 490 (1997).

[4] C. Rose-Petruck, R. Jimenez, T. Guo, A. Cavalleri, C. W. Siders, F. Raksi, J. A. Squier, B. C. Walker, K. R. Wilson, and C. P. J. Barty, Nature (London) **398**, 310 (1998).

[5] C. W. Siders, K. Sokolowski-Tinten, Cs. Toth, T. Guo, M. Kammler, M. Horn von Hoegen, K. R. Wilson, D. von der Linde, and C. P. J. Barty, Science **286**, 1340 (1999).

[6] I. Uschmann, E. Förster, P. Gibbon, C. Reich, T. Feurer, A. Morak, R. Sauerbrey, A. Rousse, P. Audebert, J.-P. Geindre, and J.-C. Gauthier (unpublished).

[7] S. Backus, C. G. Durfee III, M. M. Murnane, and H. C. Kapteyn, Rev. Sci. Instrum. **69**, 1207 (1998).

[8] F. Brunel, Phys. Rev. Lett. **59**, 52 (1987).

[9] P. Gibbon and A. R. Bell, Phys. Rev. Lett. **68**, 1535 (1992).

[10] U. Teubner, J. Bergmann, B. van Wonterghem, F. P. Schäfer, and R. Sauerbrey, Phys. Rev. Lett. **70**, 794 (1993).

[11] P. Gibbon and E. Förster, Plasma Phys. Controlled Fusion **38**, 769 (1996).

[12] J. D. Kmetec, C. L. Gordon, J. J. Macklin, B. E. Lemoff, S. G. Brown, and S. E. Harris, Phys. Rev. Lett. **68**, 1527 (1992).

[13] S. Bastiani, A. Rousse, J. P. Geindre, P. Audebert, C. Quoix, G. Hamoniaux, A. Antonetti, and J. C. Gauthier, Phys. Rev. E **56**, 7179 (1997).

[14] C. Reich, P. Gibbon, I. Uschmann, and E. Forster, Phys. Rev. Lett. **84**, 4846 (2000).

[15] C. Ziener, G. Stobrawa, H. Schwoerer, I. Uschmann, and R. Sauerbrey, Rev. Sci. Instrum. **71**, 3313 (2000).

[16] T. Missalla, I. Uschmann, E. Forster, G. Jenke, and D. von der Linde, Rev. Sci. Instrum. **70**, 1288 (1999).

[17] E. Forster, K. Gabel, and I. Uschmann, Laser Part. Beams **9**, 135 (1991).

[18] M. Krumrey, E. Tegeler, J. Barth, M. Krisch, F. Schafers, and R. Wolf, Appl. Opt. **27**, 4336 (1988).

[19] J. P. Christiansen, D. E. T. F. Ashby, and K. V. Roberts, Comput. Phys. Commun. **7**, 271 (1974).

[20] D. C. Joy, *Monte Carlo Modeling for Electron Microscopy and Microanalysis* (Oxford University Press, Oxford, 1995).

[21] E. Casnati, A. Tartari, and C. Baraldi, J. Phys. B **15**, 155 (1982).

[22] G. Zschornack, *Atomdaten für die Röntgenspektralanalyse* (Deutscher Verlag für Grund-stoffindustrie, Leipzig, 1989).

[23] A. B. Borisov, A. V. Borovskiy, V. V. Korobkin, A. M. Prokhorov, O. B. Shiryaev, X. M. Shi, T. S. Luk, A. McPherson, J. C. Solem, K. Boyer, and C. K. Rhodes, Phys. Rev. Lett. **68**, 2309 (1992).

[24] E. Esarey, P. Sprangle, J. Krall, and A. Ting, IEEE J. Quantum Electron. **33**, 1879 (1997).

[25] Y. R. Shen, *The Principles of Nonlinear Optics* (Wiley, New York, 1984).

[26] C. J. McKinstrie and D. A. Russell, Phys. Rev. Lett. **61**, 2929 (1988).

[27] M. Borghesi, A. J. MacKinnon, L. Barringer, R. Gaillard, L. A. Gizzi, C. Meyer, O. Willi, A. Pukhov, and J. Meyer-ter-Vehn, Phys. Rev. Lett. **78**, 879 (1997).

[28] A. J. Mackinnon, M. Borghesi, S. Hatchett, M. H. Key, P. K. Patel, H. Campbell, A. Schiavi, R. Snavely, S. C. Wilks, and O. Willi, Phys. Rev. Lett. **86**, 1769 (2001).

[29] J. Fuchs, G. Malka, J. C. Adam, F. Amiranoff, S. D. Baton,

N. Blanchot, A. Heron, G. Laval, J. L. Miquel, P. Mora, H. Pepin, and C. Rousseaux, Phys. Rev. Lett. **80**, 1658 (1998).

[30] A. Giulietti, A. Macchi, E. Schifano, V. Biancalana, C. Danson, D. Giulietti, L. A. Gizzi, and O. Willi, Phys. Rev. E **59**, 1038 (1999).

[31] A. Pukhov and J. Meyer-ter-Vehn, Phys. Rev. Lett. **76**, 3975 (1996).

[32] W. L. Kruer, *The Physics of Laser Plasma Interactions* (Addison-Wesley, New York, 1988).

[33] C. Gahn, G. D. Tsakiris, A. Pukhov, J. Meyer-ter-Vehn, G. Pretzler, P. Thirolf, D. Habs, and K. J. Witte, Phys. Rev. Lett. **83**, 4772 (1999).

[34] D. C. Eder, G. Pretzler, E. Fill, K. Eidmann, and A. Saemann, Appl. Phys. B: Lasers Opt. **70**, 211 (2000).